Clinical Progress

Cell Stem Cell

Circulating IGF-I and IGFBP3 Levels Control Human Colonic Stem Cell Function and Are Disrupted in Diabetic Enteropathy

Graphical Abstract

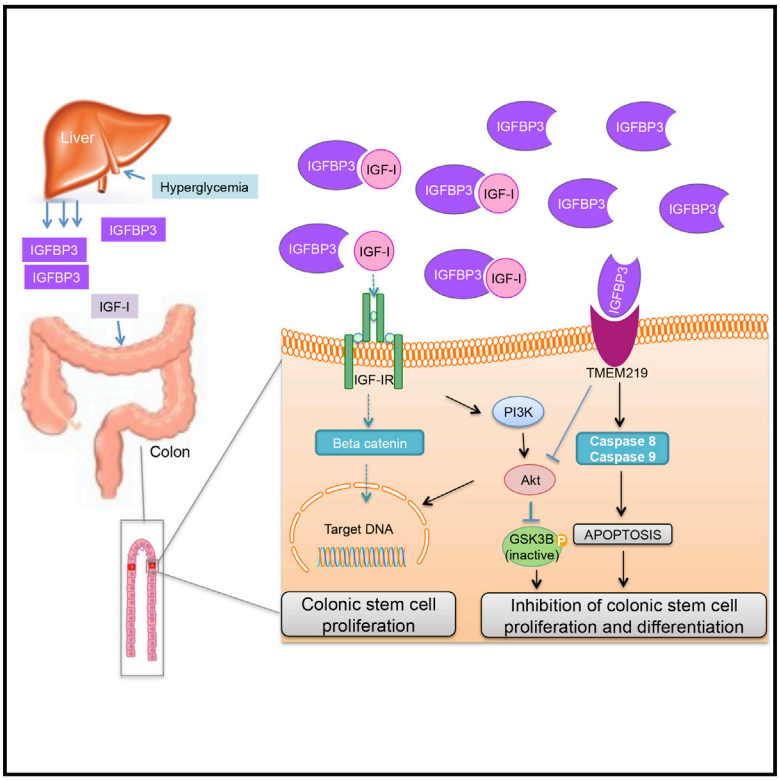

Authors

Francesca D'Addio, Stefano La Rosa, Anna Maestroni, ..., Antonio Secchi, Franco Folli, Paolo Fiorina

Correspondence

paolo.fiorina@childrens.harvard.edu

In Brief

It is unclear whether system factors regulate human colonic stem cell (CoSC) populations to control homeostasis of colonic epithelium. Now, D'Addio et al. demonstrate that circulating IGF-I/IGFBP3 controls CoSCs and represent a therapeutic target for restoring colonic function in patients with intestinal disorders arising from long-standing type 1 diabetes.

Highlights

- IGFBP3 peripheral levels are increased in T1D and diabetic enteropathy (DE)
- IGFBP3 disrupts CoSCs via a TMEM219-dependent/caspase-mediated mechanism
- Treatment of T1D restores appropriate IGFBP3 peripheral levels and improves DE
- The ecto-TMEM219 recombinant protein quenches peripheral IGFBP3 and preserves CoSCs

D'Addio et al., 2015, Cell Stem Cell *17*, 486–498
October 1, 2015
http://dx.doi.org/10.1016/j.stem.2015.07.010

CellPress

CellPress

Cell Stem Cell
Clinical Progress

Circulating IGF-I and IGFBP3 Levels Control Human Colonic Stem Cell Function and Are Disrupted in Diabetic Enteropathy

Francesca D'Addio,[1,2,15] Stefano La Rosa,[3,15] Anna Maestroni,[2] Peter Jung,[4] Elena Orsenigo,[5] Moufida Ben Nasr,[1,2] Sara Tezza,[1,2] Roberto Bassi,[1,2] Giovanna Finzi,[3] Alessandro Marando,[3] Andrea Vergani,[1,2] Roberto Frego,[6] Luca Albarello,[7] Annapaola Andolfo,[8] Roberta Manuguerra,[9] Edi Viale,[6] Carlo Staudacher,[5] Domenico Corradi,[9] Eduard Batlle,[4,10] David Breault,[11] Antonio Secchi,[2,12] Franco Folli,[13,14] and Paolo Fiorina[1,2,*]

[1]Nephrology Division, Boston Children's Hospital, Harvard Medical School, Boston, MA 02115, USA
[2]Transplant Medicine, IRCCS Ospedale San Raffaele, Milan 20132, Italy
[3]Department of Pathology, Ospedale di Circolo, Varese 21100, Italy
[4]Institute for Research in Biomedicine (IRB Barcelona), Barcelona 08028, Spain
[5]Surgery
[6]Gastroenterology
[7]Pathology Unit
[8]ProMiFa, Protein Microsequencing Facility
IRCCS Ospedale San Raffaele, Milan 20132, Italy
[9]Department of Biomedical, Biotechnological and Translational Sciences, Unit of Pathology, University of Parma, Parma 43121, Italy
[10]Institució Catalana de Recerca i Estudis Avançats (ICREA), Barcelona 08028, Spain
[11]Division of Endocrinology, Boston Children's Hospital, Harvard Medical School, Boston, MA 02115, USA
[12]Vita Salute San Raffaele University, Milano 20132, Italy
[13]Department of Medicine, Division of Diabetes, University of Texas Health Science Center at San Antonio, San Antonio, TX 78229, USA
[14]Department of Internal Medicine, Obesity and Comorbidities Research Center (O.C.R.C.), State University of Campinas, São Paulo 13100, Brazil
[15]Co-first author
*Correspondence: paolo.fiorina@childrens.harvard.edu
http://dx.doi.org/10.1016/j.stem.2015.07.010

SUMMARY

The role of circulating factors in regulating colonic stem cells (CoSCs) and colonic epithelial homeostasis is unclear. Individuals with long-standing type 1 diabetes (T1D) frequently have intestinal symptoms, termed diabetic enteropathy (DE), though its etiology is unknown. Here, we report that T1D patients with DE exhibit abnormalities in their intestinal mucosa and CoSCs, which fail to generate in vitro mini-guts. Proteomic profiling of T1D+DE patient serum revealed altered levels of insulin-like growth factor 1 (IGF-I) and its binding protein 3 (IGFBP3). IGFBP3 prevented in vitro growth of patient-derived organoids via binding its receptor TMEM219, in an IGF-I-independent manner, and disrupted in vivo CoSC function in a preclinical DE model. Restoration of normoglycemia in patients with long-standing T1D via kidney-pancreas transplantation or in diabetic mice by treatment with an ecto-TMEM219 recombinant protein normalized circulating IGF-I/IGFBP3 levels and reestablished CoSC homeostasis. These findings demonstrate that peripheral IGF-I/IGFBP3 controls CoSCs and their dysfunction in DE.

INTRODUCTION

Gastrointestinal disorders, consisting of gastroparesis, abdominal distension, irritable bowel syndrome, and fecal incontinence, are common in individuals with type 1 diabetes (T1D) (The Diabetes Control and Complications Trial Research Group, 1993). Indeed, up to 80% of individuals with long-standing T1D, who are generally affected by several diabetic complications including end stage renal disease (ESRD) (The Diabetes Control and Complications Trial Research Group, 1993; Atkinson et al., 2014; Fiorina et al., 2001), show intestinal symptoms. The presence of these gastrointestinal symptoms, known as diabetic enteropathy (DE), significantly reduces the quality of life (The Diabetes Control and Complications Trial Research Group, 1993; Atkinson et al., 2014; Camilleri, 2007; Talley et al., 2001) and has a largely unknown pathogenesis (Feldman and Schiller, 1983). Preclinical studies showed significant derangement of the intestinal mucosa morphology in diabetic rodents (Domènech et al., 2011; Zhao et al., 2003), suggesting that in T1D, intestinal homeostasis may be altered; however, little data are available in humans. The intestinal epithelium is maintained by intestinal stem cells and their niche, which respond to physiological stress and to environmental injury (Barker, 2014; Medema and Vermeulen, 2011). Colonic stem cells (CoSCs), located at the crypt base of the large intestine and expressing the ephrin B receptor 2 (EphB2), leucine-rich repeat containing G protein-coupled receptor 5 (LGR5), human telomerase reverse transcriptase (h-TERT), and aldehyde dehydrogenase (Aldh), among other

markers (Carlone and Breault, 2012; Carpentino et al., 2009; Jung et al., 2011; Sato and Clevers, 2013), constitute, together with the local microenvironment, the CoSC niche (van der Flier and Clevers, 2009; Zeki et al., 2011). Recent studies have established conditions that recapitulate many features of intestinal homeostasis and generate normal self-renewing crypt organoids in vitro, or so-called "mini-guts" (Jung et al., 2011; Sato and Clevers, 2013; Sato et al., 2011). Whether systemic factors, such as circulating hormones, serve to control CoSCs remains to be established (Stange and Clevers, 2013). We hypothesize that a dyad consisting of a circulating enterotrophic regulating factor and its binding protein (insulin-like growth factor 1 (IGF-I), and its binding protein 3, IGFBP3) finely controls CoSCs and becomes dysfunctional in DE. Here we demonstrate that individuals with long-standing T1D and DE have altered CoSCs and show increased circulating levels of IGFBP3. Administration of IGFBP3 alters CoSC self-renewal potential and mucosal morphology in vitro and in vivo, in a preclinical model of DE, by quenching circulating IGF-I and by exerting a TMEM219-dependent/caspase-mediated toxic effect on CoSCs. Finally, targeting IGFBP3 with the newly generated ecto-TMEM219 recombinant protein, based on the extracellular domain of the IGFBP3 receptor (TMEM219), abrogates IGFBP3 deleterious effects in vitro and in vivo.

RESULTS

Intestinal Dysfunction and Clinical Symptoms Are Present in Long-Standing T1D

We first characterized intestinal morphology and function in a population of individuals with long-standing T1D and end stage renal disease (T1D+ESRD) and in healthy subjects (CTRL). Severe intestinal symptoms, such as diarrhea, abdominal pain, and constipation were evident in T1D+ESRD individuals as assessed using the Gastrointestinal Symptom Rating Scale (GSRS) questionnaire (Figures 1A–1C). Symptoms were associated with abnormalities in anorectal sphincter function (Figures 1D–1F). The intestinal mucosa was altered in individuals with T1D+ESRD as compared to healthy subjects, with lower numbers of crypts, distortion, and zonal sclerosis of the lamina propria (Figures 1G1–1H). A significant reduction in epithelial cell proliferation as assessed by MKI67 (MIB1 antibody) staining (Figures 1I1–1J), signs of neural degeneration, and reduction in serotonin expression in intestinal neuroendocrine cells (Figures 1K–1N) were observed, confirming the presence of DE in these individuals.

CoSCs Are Altered in Long-Standing T1D

The characterization of colonic crypts revealed a significant reduction in EphB2^{+} expression and in the number of aldehyde dehydrogenase (Aldh)$^{+}$ immunoreactive cells, both markers of local stem cells (Carpentino et al., 2009; Jung et al., 2011), in T1D+ESRD individuals as compared to healthy subjects (Figures 1O–1R). A profound decrease was evident, upon gating on viable cells at FACS analysis (Figures S1A–S1C), in the percentage of EphB2^{hi}, EphB2^{hi+}LGR5^{+}, and EphB2^{+}h-TERT^{+} cells isolated from intestinal crypts obtained from T1D+ESRD individuals as compared to healthy subjects (Figures 2A–2E; Figures S1D and S1E) and was confirmed by RT-PCR (Figures 2F–2H) and western blot (WB) analysis (Figure S1F). Transcriptome profiling of crypts obtained from T1D+ESRD documented decreased expression in Notch pathway (*NOTCH1* and *2*, *JAG1*, *DLL1*, and *SOX1* and *2*), Wnt pathway (*APC*, *FZD1*, *DKC1*, *ETS2*, *FAM84A*, *GPX2*, and *RNF43*), and BMP pathway (*BMP1*, *BMP2*, and *BMP3*) genes, previously known pathways that control CoSCs, as compared to the expression of these genes in healthy subjects (Figure S1G and Table S1). Analysis of CoSC signature genes revealed that *LGR5*, *EPHB2* (Gracz et al., 2013; Merlos-Suárez et al., 2011), h-*TERT* (Breault et al., 2008), and other intestinal stem cell marker genes (Hughes et al., 2011; Muñoz et al., 2012; Ziskin et al., 2013) were significantly underexpressed in T1D+ESRD as compared to healthy subjects as well (Figure 2I), confirming that CoSCs are altered in individuals with DE.

In Vitro Generation of Mini-Guts Is Altered in Long-Standing T1D

In order to evaluate CoSC self-renewal properties, we used the in vitro mini-gut assay. Indeed, crypts isolated from T1D+ESRD individuals and cultured in vitro for 8 days formed small spheroid mini-guts that failed to grow as compared to those from healthy subjects (Figures 2J1–2K), despite a comparable viability (Figures S1H and S1I) and efficiency of forming mini-guts in both groups (Figure S1J). To begin to elucidate the effect of circulating factors and high glucose on CoSCs, we cultured isolated intestinal crypts (obtained from either healthy subjects or long-standing T1D individuals) in high glucose with/without serum in vitro for 8 days (Figures 2L–2M). High glucose partially prevented the generation of fully mature mini-guts and synergized with serum of long-standing T1D individuals in altering CoSC self-renewal properties, such that mini-guts appeared collapsed (Figures 2L2–2L4). Analysis of gene expression also revealed changes in the CoSC signature (Figure 2N), thus suggesting that hyperglycemia and circulating factors act together to alter CoSC self-renewal properties in long-standing T1D.

Serum Unbiased Proteomic Profiling Revealed Increased Levels of IGFBP3 in Long-Standing T1D

In order to identify potential circulating factors that may serve as enterotrophic hormones and may have a role in regulating CoSCs, we compared the serum proteome of healthy subjects with T1D+ESRD individuals using an unbiased proteomic approach. A clear proteomic profile was evident in T1D+ESRD individuals as compared to healthy subjects, with more than 50% of the detected proteins segregating in either one group or the other (Figure 3A). Some proteins were associated with diabetes, and some were growth factors or stem cell-related proteins or were potentially involved in intestinal functions (Figure 3A). In particular, the levels of IGF-I binding proteins (IGFBP2 and 3) were detectable in long-standing T1D individuals as compared to healthy subjects, with IGFBP3 almost 5-fold increased (Figure 3B), while IGFBP1, 4, 5, and 6 remained almost undetectable. Interestingly, in the liver of individuals with long-standing T1D, hepatocytes, but not Kupffer cells, showed a higher IGFBP3 immunohistochemical expression as compared to healthy subjects (Figures 3C1 and 3C2; Figures S1K–S1L), suggesting an increase in IGFBP3 hepatic synthesis and release. The effect of high glucose on IGFBP3 hepatic release was confirmed by the detection of increased IGFBP3 levels in the supernatant of human immortalized hepatocytes exposed to

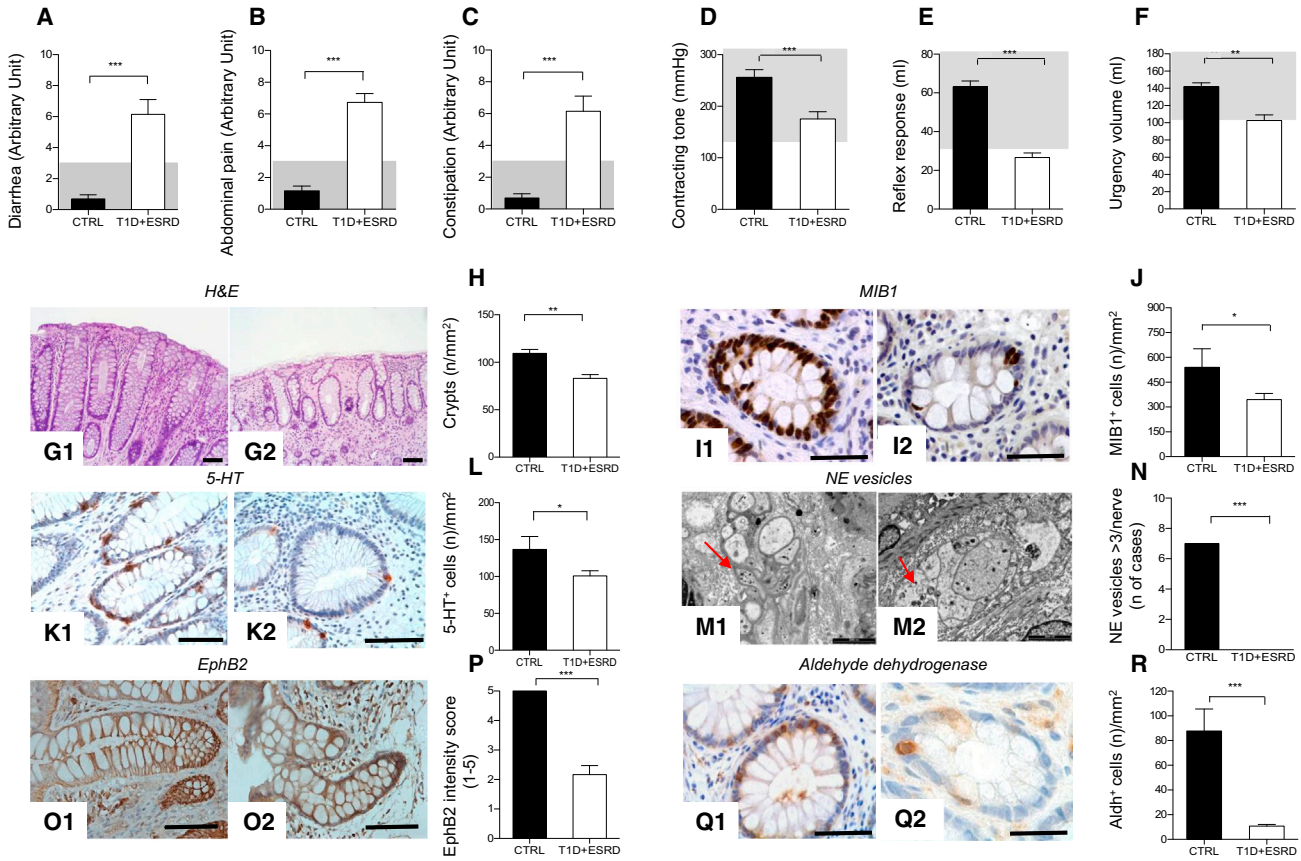

Figure 1. DE in Long-Standing T1D Is Characterized by Intestinal Mucosa Abnormalities and Impairment in CoSCs

(A–C) Bar graphs depict the score of diarrhea, abdominal pain, and constipation according to the administration of the GSRS questionnaire in healthy subjects (CTRL) and long-standing T1D individuals (T1D+ESRD). Gray area indicates normal range for the parameter.

(D–F) Bar graphs report the measurements of anorectal sphincter contracting tone (mmHg), reflex response (ml), and urgency volume (ml) by anorectal manometry in healthy subjects (CTRL) and long-standing T1D individuals (T1D+ESRD). Gray area indicates normal range for the parameter. n = 20 CTRL and n = 60 T1D+ESRD individuals were included in the evaluation.

(G1, G2, I1, I2, K1, K2, M1, M2, O1, O2, Q1, and Q2) Representative images of H&E histology staining, immunoreactive MKI67$^+$ cells (MIB1$^+$), ultrastructural analysis of neural structures with red arrows indicating localization and presence of neuroendocrine vesicles, immunohistochemical expression of 5-HT, aldehyde dehydrogenase (Aldh)$^+$ cells, and EphB2$^+$ expression on bioptic samples obtained from healthy subjects (CTRL; G1, I1, K1, M1, O1, and Q1) and long-standing T1D individuals (T1D+ESRD; G2, I2, K2, M2, O2, and Q2). Ultrastructural analysis scale bar, 2,000 nm. Original histology magnification: 100× in (G1) and (G2); 400× in (I1), (I2), (K1), and (K2); 40× in (O1) and (O2); 200× in (Q1) and (Q2). Scale bar, 80 μm.

(H, J, L, N, P, and R) Bar graphs reporting the measurement of crypts, the number of MKI67$^+$ (MIB1$^+$) cells, the number of neuroendocrine vesicles of nerve terminals (number of cases with >3 NE vesicles detected per nerve terminal), the number of 5-HT$^+$ and Aldh$^+$ cells, and the of EphB2$^+$ expression (intensity score 0–5) in CTRL and long-standing T1D subjects (T1D+ESRD). n = 20 CTRL and n = 60 T1D+ESRD individuals were included in the evaluation. Data are expressed as mean ± SEM unless differently reported. *p < 0.01; **p < 0.001; ***p < 0.0001.

GSRS, Gastrointestinal Symptom Rating Scale; T1D, type 1 diabetes; ESRD, end stage renal disease; CTRL, healthy subjects; MIB1, antibody against MKI67; EphB2, Ephrin B receptor 2; Aldh, aldehyde dehydrogenase; 5-HT, serotonin; NE, neuroendocrine vesicles.

high glucose (Figure 3D). Finally, serum levels of free IGF-I appeared significantly reduced in long-standing T1D as compared to healthy subjects (Figure 3E), indicating that circulating IGF-I and IGFBP3 levels are altered in long-standing T1D.

Peripheral IGFBP3 and IGF-I Control CoSCs

To further elucidate the role of circulating IGF-I and IGFBP3 in the regulation of the CoSCs and of intestinal epithelial proliferation, we demonstrated the expression of IGF-I receptor (IGF-IR) and of IGFBP3 receptor (TMEM219) on isolated crypts (Figures 3F–3H; Figures S1M–S1N) using RT-PCR and WB, and we confirmed the expression of IGF-IR on CoSCs with immunostaining (Figures S1N1 and S1N2) and that of TMEM219 with in situ hybridization (Figures 3G1 and 3G2). In order to mechanistically confirm the role of IGF-I and IGFBP3 on CoSCs, we tested the effect of several molecules, identified by proteomic profiling, in our in vitro mini-gut assay. Our strategy to select potential targets is reported in the Supplemental Information. The severely altered mini-guts generated from intestinal samples obtained from T1D+ESRD individuals were rescued by the addition of recombinant human IGF-I (IGF-I) to the culture medium (Figure 3I), while the addition of recombinant human IGFBP3 (IGFBP3) resulted in the abrogation of the positive effect observed with IGF-I, with a decreased development of mini-guts and increased

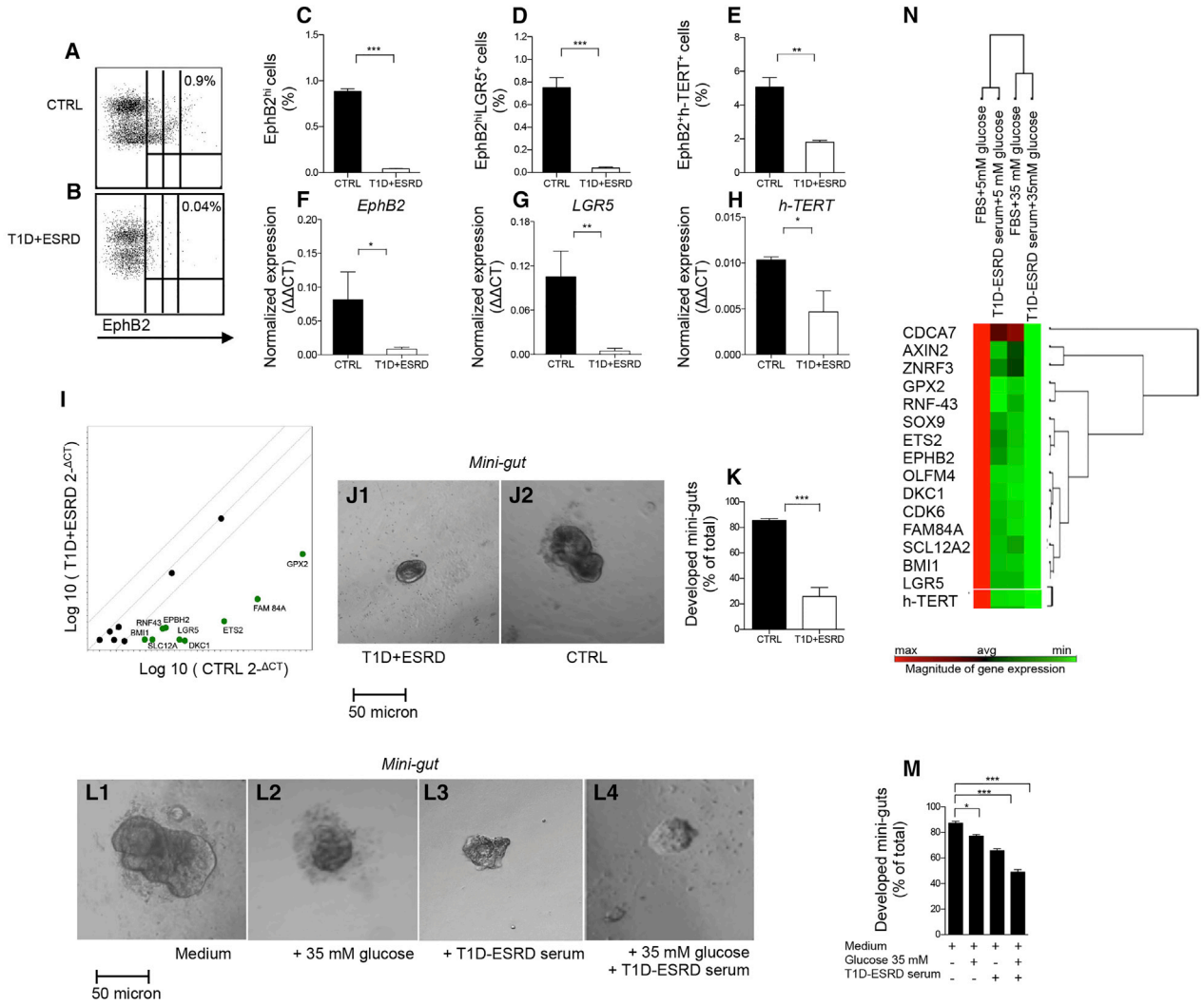

Figure 2. DE in Long-Standing T1D Is Associated with a Defect in CoSCs

(A and B) Representative flow dot plots of EphB2^{low}, EphB2^{medium}, and EphB2^{hi} cells in healthy subjects (CTRL) and long-standing T1D individuals (T1D+ESRD).

(C–E) Bar graphs depict results of flow cytometric analysis of EphB2^{hi+}, EphB2^{hi+}LGR5^{+}, and EphB2^{+}h-TERT^{+} cells in freshly isolated crypts (n = 10 CTRL and n = 10 T1D+ESRD).

(F–H) Bar graphs depict expression data of CoSC markers *EphB2*, *LGR5*, and h-*TERT* as normalized mRNA expression measured by RT-PCR on isolated intestinal crypts. All samples were run in triplicate and normalized to expression of the housekeeping gene *ACTB* (ΔΔCt).

(I) Scatter plot represents the CoSC signature markers and stem cell transcriptome profiling examined in freshly isolated intestinal crypts of n = 10 healthy subjects (CTRL) and n = 10 long-standing T1D individuals (T1D+ESRD).

(J1 and J2) Representative images of mini-guts cultured for 8 days in vitro obtained from previously isolated crypts of long-standing T1D individuals (T1D+ESRD) and healthy subjects (CTRL). 10× magnification. Scale bar, 50 μm.

(K) Bar graph depicts the percentage of developed mini-guts of the total at 8 days of culture of freshly isolated intestinal crypts from n = 10 CTRL and n = 10 T1D+ESRD individuals.

(L1–L4) Representative images of mini-guts obtained from previously isolated crypts of healthy subjects (CTRL) and cultured for 8 days in the following conditions: L1 = normal (FBS) serum+normal glucose (5 mM); L2 = T1D+ESRD serum+normal glucose; L3 = normal serum+high glucose (35 mM); L4 = T1D+ESRD serum+high glucose. 10× magnification. Scale bar, 50 μm.

(M) Bar graph grouping percentage of developed mini-guts of the total at 8 days of culture from freshly isolated intestinal crypts cultured with the following conditions: normal (FBS) serum+normal glucose (5 mM); T1D+ESRD serum+normal glucose; normal serum+high glucose (35 mM); T1D+ESRD serum+high glucose. Statistical significance has been calculated within each group (normal glucose+normal serum, medium+high glucose, medium+long-standing T1D serum, and high glucose+long-standing T1D serum) by comparing different culturing conditions. Comparison in the bar graph refers to all conditions versus normal serum+normal glucose.

(N) Transcriptome profiling depicting CoSC-signature marker expression in isolated crypts obtained from healthy subjects and cultured with/without high glucose and/or long-standing T1D serum. n = 10 subjects per group were evaluated. Data are expressed as mean ± SEM unless differently reported. *p < 0.01; **p < 0.001; ***p < 0.0001. See also Figure S1.

CoSC, colonic stem cell; T1D, type 1 diabetes; ESRD, end stage renal disease; CTRL, healthy subjects; EphB2, Ephrin B receptor 2; LGR5, leucine-rich repeat containing G protein-coupled receptor 5; RT-PCR, real-time polymerase chain reaction; ACTB, beta actin; FBS, fetal bovine serum.

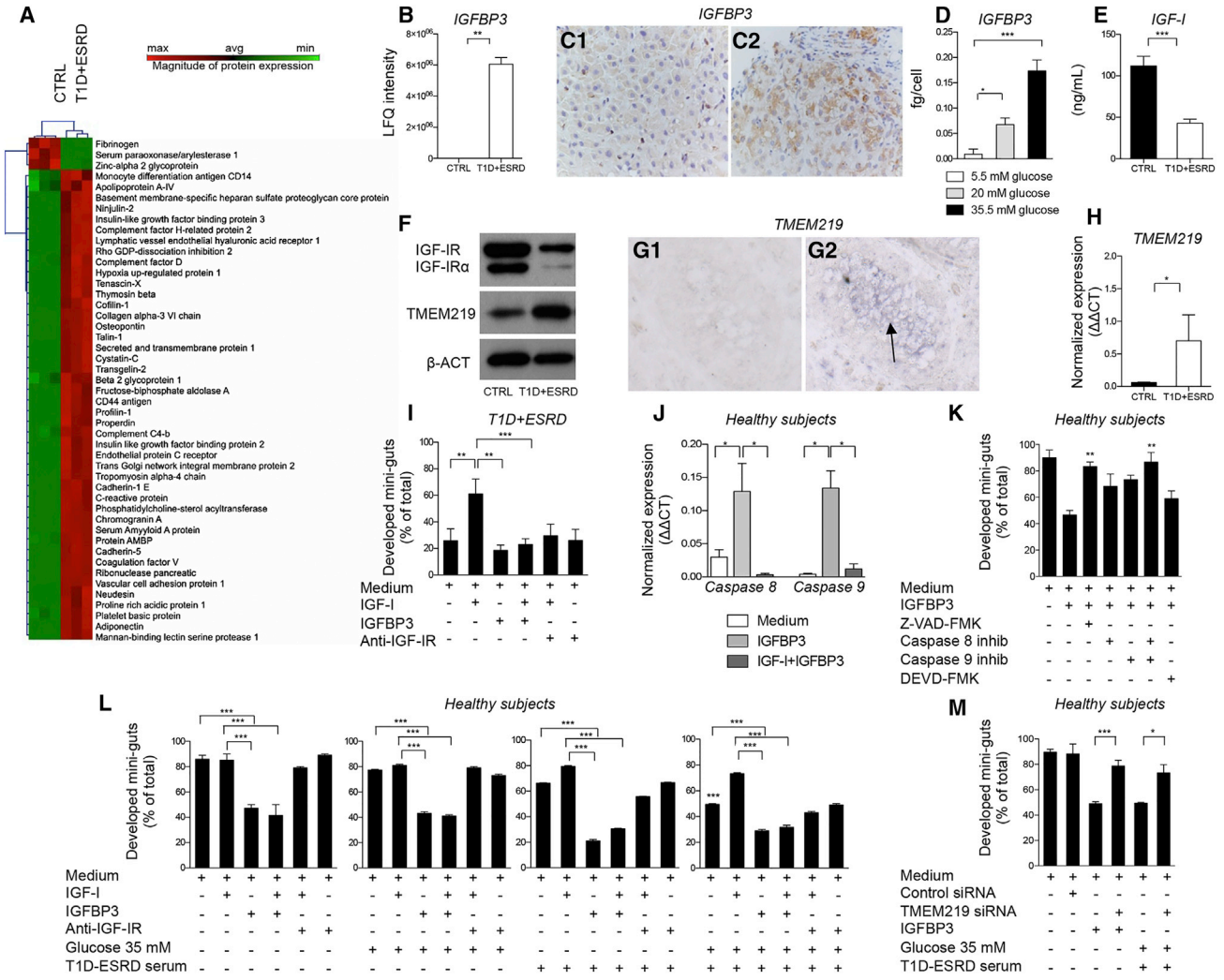

Figure 3. Circulating IGF-I and IGFBP3 Are Altered in Long-Standing T1D and Its Manipulation in Vitro Induces Profound Effects on CoSC Growth and Self-Renewal

(A) Heat map represents the proteomic profile in long-standing T1D (T1D+ESRD) as compared to healthy subjects (CTRL). The complete dataset of identified and quantified proteins was subjected to statistical analysis ($p < 0.01$). Significantly differentially expressed proteins were further analyzed through hierarchical clustering. Sera of n = 10 CTRL and n = 10 T1D+ESRD individuals were analyzed.

(B) Bar graph depicts LFQ intensity for a single protein extrapolated from the untargeted proteomic analysis, insulin-like growth factor binding protein 3 (IGFBP3).

(C1 and C2) Representative images (40× magnification) of IGFBP3 expression in the liver. IGFBP3 is mildly and diffusely expressed in the liver parenchyma from healthy subjects (C1), while it is more zonally positive in long-standing diabetic individuals (C2).

(D) Bar graph represents IGFBP3 levels measured by ELISA in the supernatants of immortalized human hepatoma cell line (HuH-7) cultured for 5 days at different glucose concentrations (35 mM: high glucose; 20 mM: intermediate glucose; 5 mM: normal glucose). Experiments were performed in triplicate.

(E) Bar graph represents insulin-like growth factor 1 (IGF-I) levels measured by ELISA in serum of healthy subjects and long-standing T1D (T1D+ESRD).

(F) WB analysis (cropped blots) confirmed IGF-IR and TMEM219 expression on the intestinal crypt surface. Evaluation of total IGF-IR expression by WB includes the detection of IGF-IRα, a subunit of IGF-IR whole protein.

(G1 and G2) Representative pictures of TMEM219 in situ hybridization (G1, negative control; G2, TMEM219 staining) performed on rectal mucosa biopsy samples obtained from CTRL. 20× magnification.

(H) Bar graph depicts normalized mRNA expression of *TMEM219* (IGFBP3 receptor) using the ΔΔCt method. n = 5 subjects per group were evaluated.

(I) Bar graph grouping percentage of developed mini-guts of the total obtained from long-standing T1D individuals in different conditions and showing the effect of IGF-I, IGFBP3, and anti-IGF-IR. The p values are relative to baseline conditions and addition of IGF-I to culture.

(J) Bar graph representing normalized mRNA expression of *caspase 8* and *caspase 9* in crypts isolated from healthy subjects cultured in the presence of IGFBP3 and IGF-I+IGFBP3. Experiments were performed in triplicate.

(K) Bar graph grouping percentages of developed mini-guts of the total at 8 days of culture, obtained from healthy subjects and cultured in the presence of a pan-caspase inhibitor or selective inhibitors of caspases 8, 9, and 3 and IGFBP3. Assay was performed in triplicate.

(L) Bar graphs grouping percentages of developed mini-guts of the total obtained from healthy subjects and cultured in different conditions (normal glucose+normal serum, high glucose+normal serum, T1D+ESRD serum+normal glucose, and T1D+ESRD serum+high glucose) and showing the effects of IGF-I, IGFBP3, and anti-IGF-IR. The p values are relative to the baseline condition (medium alone, medium+high glucose, medium+long-standing T1D serum, and high

(legend continued on next page)

formation of collapsed and distorted organoids (Figure 3I). Because IGFBP3 has been recently shown to act independently of IGF-I (Williams et al., 2007) via the IGFBP3 receptor (TMEM219) (Baxter, 2013), it was necessary to clarify whether IGFBP3 exerts its effects on CoSCs by binding IGF-I or by directly targeting TMEM219 on CoSCs. We first confirmed that IGFBP3 has a direct pro-apoptotic effect on CoSCs by demonstrating increased *caspse 8* and *caspse 9* expression in mini-guts obtained from healthy subjects and long-standing T1D individuals and cultured with IGFBP3 (Figure 3J; Figures S2A and S2B), while the addition of a pan-caspase inhibitor (Z-VAD-FMK) or both selective inhibitors of caspases 8 and 9, but not the addition of caspase 3 inhibitor, abrogated the IGFBP3 effect (Figure 3K). We then demonstrated that the addition of IGF-I did not rescue the development of mini-guts obtained from healthy subjects and exposed to IGFBP3 (Figure 3L), confirming that IGFBP3 may act through both a direct and an indirect IGF-I mechanism. Interestingly, high glucose alone was unable to completely disrupt mini-gut growth, and anti-IGF-IR did not worsen growth and morphology of mini-guts formed from healthy subjects (Figure 3L). The addition of IGF-I to mini-guts generated from healthy subjects, but cultured with high glucose and serum from long-standing T1D individuals, rescued mini-gut morphology, while IGFBP3 abolished the positive effect of IGF-I when added to the mini-gut culture (Figure 3L). Interestingly, the use of healthy subjects' "CTRL" serum in culturing crypts obtained from long-standing T1D nearly restored mini-gut development/morphology, indicating that circulating factors, and in particular the IGF-I/IGFBP3 dyad, control CoSCs (Figures S2C and S2D). We then genetically modulated *TMEM219* expression by using siRNA in vitro in mini-guts obtained from healthy subjects. Knockdown of TMEM219 in mini-guts preserved their ability to grow and self-renew, despite the addition of IGFBP3 and high glucose with long-standing T1D serum (Figure 3M). Concomitant blockade of TMEM219 by siRNA and antibody blockade of IGF-IR did not result in any additional beneficial effect on mini-gut development despite our using serum from healthy subjects or from long-standing T1D (Figure S2E).

Other circulating proteins that appeared altered in the serum proteome of long-standing T1D individuals were tested in the in vitro mini-gut assay and did not show any significant effect on mini-gut growth (Figures S2F and S2G). C-peptide and insulin, which are commonly altered in T1D and which may interfere with the IGF-I/IGFBP3 dyad by binding IGF-IR (Figures S2F–S2H), were tested as well and did not show any effect.

To further confirm that the IGF-I/IGFBP3 dyad effectively targets CoSCs and not only crypts, we tested the effect of IGF-I/IGFBP3 on single-cell-derived mini-guts. We flow-sorted EphB2$^+$ cells from isolated crypts and established that *TMEM219* was highly expressed on their surface (Figure 4A). We then cultured EphB2$^+$ cells in the in vitro single-cell-derived mini-gut assay and confirmed that high glucose and long-standing T1D serum exposure as well as the addition of IGFBP3 significantly abrogated single-cell-derived mini-gut growth, thus recapitulating the primary features reported in our previous observations on crypt-derived mini-guts (Figure 4B, Figures S3A1–S3A3). Moreover, expression of *caspase 8* and *caspase 9* was upregulated in IGFBP3-treated mini-guts and in those exposed to high glucose and long-standing T1D serum, while *MKI67*, a marker of proliferation, was significantly underexpressed (Figures S3B–S3D).

Effect of the IGF-I/IGFBP3 Dyad on Previously Known Pathways that Control CoSCs

In order to clarify the effects of the IGF-I/IGFBP3 dyad on pathways previously known to be involved in CoSC niche function (i.e., Wnt/Notch/BMP), we obtained from our stem cell transcriptome profile the expression of niche-regulating specific gene transcripts. IGF-I restores the expression of some factors associated with Wnt/Notch signaling pathways on mini-guts obtained from crypts of T1D+ESRD (Figure S3E, Table S2), while IGFBP3 poorly affects Wnt/Notch/BMP gene expression in mini-guts obtained from crypts of healthy subjects or from those obtained from T1D+ESRD individuals (Figure S3F, Table S2). This confirms that IGF-I preserves the expression of some genes involved in Wnt/Notch/BMP signaling, but also that IGFBP3 acts independently on CoSCs, without major alterations in the expression of key target genes of the other previously known pathways.

Effect of the IGF-I/IGFBP3 Dyad on Apoptotic Pathways

An extensive transcriptome analysis performed to clarify the IGFBP3 caspase-mediated effect on mini-guts (Figures 4C and 4D; Figures S3G and S3H, Table S3) showed that the addition of IGFBP3 to mini-guts grown from healthy subject crypts was associated with a significant upregulation of caspase cascade activators (*caspase 8* and *caspase 9*) and pro-apoptotic genes, while the anti-apoptotic gene *BCL2* was downregulated (Figure 4C). Interestingly, anti-apoptotic genes (*BCL2*, *FAS*, and *NOL3*) were significantly underexpressed in mini-guts grown from T1D+ESRD crypts as well, as compared to healthy subjects, while the majority of caspase-related genes (*caspase 1, 5, 7, 8, 9,* and *14*) were overexpressed (Figure S3G). Moreover, the expression of genes involved in other pro-apoptotic pathways was either not altered (i.e., *FASL*, *FADD*, and *TNF*) or inhibited (*TRADD*) in T1D+ESRD mini-guts. The opposite effect was observed when IGF-I was added (Figure 4D; Figure S3H). The absence of alterations in the expression of oxidative stress target genes (data not shown), and the absence of any effect of oxidative stress factors (Figures S3I and S3J), confirmed

glucose+long-standing T1D serum). Additional p values have been calculated to compare the difference in mini-gut growth among the following conditions: medium alone versus medium+high glucose versus medium+high glucose+long-standing T1D serum. Assay was performed in triplicate.

(M) Bar graph grouping percentages of developed mini-guts of the total obtained from healthy subjects, cultured for 8 days, and exposed to TMEM219 targeting with siRNA, compared to TMEM219-expressing crypts in medium alone and in medium+high glucose+long-standing T1D serum. Assay was performed in triplicate. Data are expressed as mean ± SEM unless differently reported. *p < 0.01; **p < 0.001; ***p < 0.0001. See also Figures S1 and S2.

IGF-I, insulin-like growth factor 1; IGFBP3, insulin-like growth factor binding protein 3; IGF-IR, insulin-like growth factor 1 receptor; CoSC, colonic stem cell; T1D, type 1 diabetes; ESRD, end stage renal disease; CTRL, healthy subjects; RT-PCR, real-time polymerase chain reaction; ACTB, beta actin; LFQ, label-free quantitation; SEM, standard error of the mean; siRNA, small RNA interference; inhib, inhibitor.

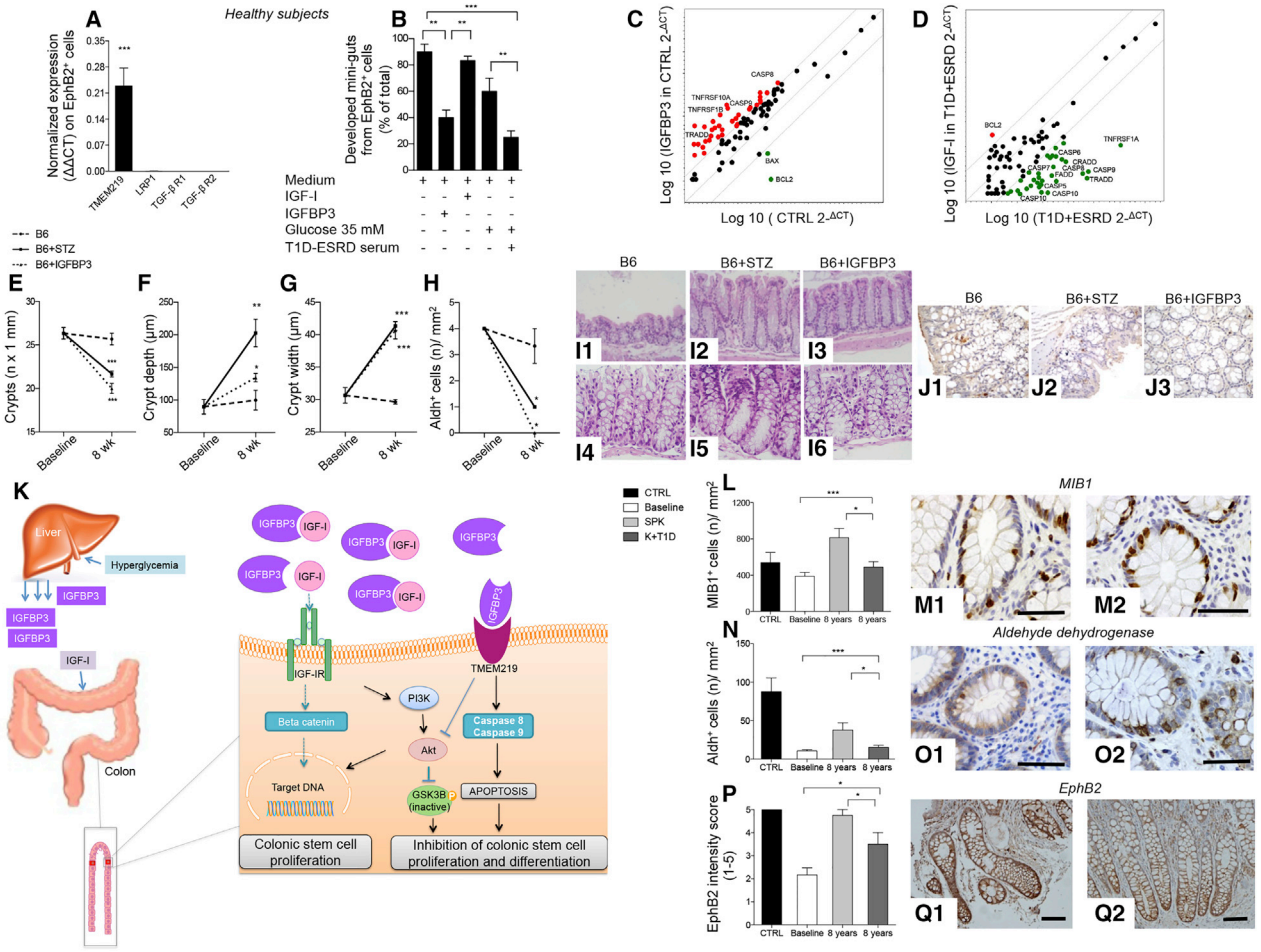

Figure 4. Effects of the Peripheral IGF-I/IGFBP3 Dyad on Single-Cell-Derived In Vitro Mini-Guts and the caspase Cascade

Manipulating the peripheral IGF-I/IGFBP3 dyad alters the progression of diabetic enteropathy in a preclinical model of diabetic enteropathy, while the treatment of long-standing T1D with simultaneous pancreas-kidney transplantation (SPK) ameliorates intestinal symptoms, motility, and morphology.

(A) Bar graph representing normalized mRNA expression of *TMEM219, LRP1,* and *TGF-β type I* and *II* in EphB2$^+$ sorted single cells obtained from crypts of healthy subjects. Experiments were performed in triplicate.

(B) Bar graphs showing percentages of developed single-cell-derived mini-guts (of the total) obtained from EphB2$^+$ cells sorted from freshly isolated crypts of healthy subjects and cultured in different conditions (normal glucose+normal serum, high glucose+normal serum, T1D+ESRD serum+normal glucose, and T1D+ESRD serum+high glucose) and showing the effect of IGF-I and IGFBP3. The p values are relative to baseline conditions.

(C and D) Scatter plot representing the apoptosis transcriptome profiling examined in freshly isolated intestinal crypts of healthy subjects (CTRL) and long-standing T1D individuals (T1D+ESRD) cultured with/without IGFBP3 and IGF-I. Experiments were performed in triplicate.

(E–G) Line graphs reporting the number of crypts (E), depth of crypts (F), and width of crypts (G) assessed on intestinal lower tract sections harvested at baseline and after 8 weeks from STZ-treated B6 mice developing DE (B6+STZ), naive B6 (B6), and naive B6 treated with IGFBP3 (B6+IGFBP3). STZ, streptozoticin-treated. n = 3 mice per group were evaluated.

(H) Bar graph representing the number of Aldh$^+$ cells/mm^2 in immunostained sections of STZ-treated B6 mice developing DE, B6, and naive B6 treated with IGFBP3 (B6+IGFBP3).

(I1–I6) Representative images of intestinal crypts on H&E sections of B6, B6+STZ mice developing DE, and naive B6 treated with IGFBP3 (B6+IGFBP3). Histology magnification, 200× in (I1)–(I3) and 400× in (I4)–(I6).

(J1–J3) Representative images of Aldh$^+$ cells on immunostained sections of intestinal lower tract harvested from STZ-treated B6 mice developing DE, B6, and naive B6 treated with IGFBP3 (B6+IGFBP3). Histology magnification, 400×.

(K) Schematic attempt to represent the effect of circulating IGF-I and IGFBP3 on CoSCs.

(L, N, and P) Bar graphs report the measurement of MIB1$^+$ and Aldh$^+$ cells and EphB2$^+$ expression (intensity score 0–5) in the four groups of subjects (n = 20 CTRL, n = 30 SPK, n = K+T1D, and n = 60 T1D+ESRD).

(M1, M2, O1, O2, Q1, and Q2) Representative images of MIB1$^+$ and Aldh$^+$ cells, and EphB2$^+$ expression in immunostained rectal mucosa bioptic samples of T1D+ESRD who underwent kidney transplant alone (K+T1D) or SPK transplantation at 8 years of follow-up. Histology magnification, 400× in (M1), (M2), (O1), and (O2), 20× in (Q1) and (Q2). Scale bar, 80 μm. Data are expressed as mean ± SEM unless differently reported. *p < 0.01; **p < 0.001; ***p < 0.0001. See also Figures S3, S4, and S5.

STZ, streptozoticin-treated; B6, C57BL/6J mice; IGF-I, insulin-like growth factor 1; IGFBP3, insulin-like growth factor binding protein 3; IGF-IR, insulin-like growth factor 1 receptor; CoSC, colonic stem cell; T1D, type 1 diabetes; ESRD, end stage renal disease; CTRL, healthy subjects; SPK, simultaneous kidney-pancreas transplantation; K+T1D, kidney transplantation alone in type 1 diabetes; MIB1, antibody against MKI67; EphB2, Ephrin B receptor 2; Aldh, aldehyde dehydrogenase.

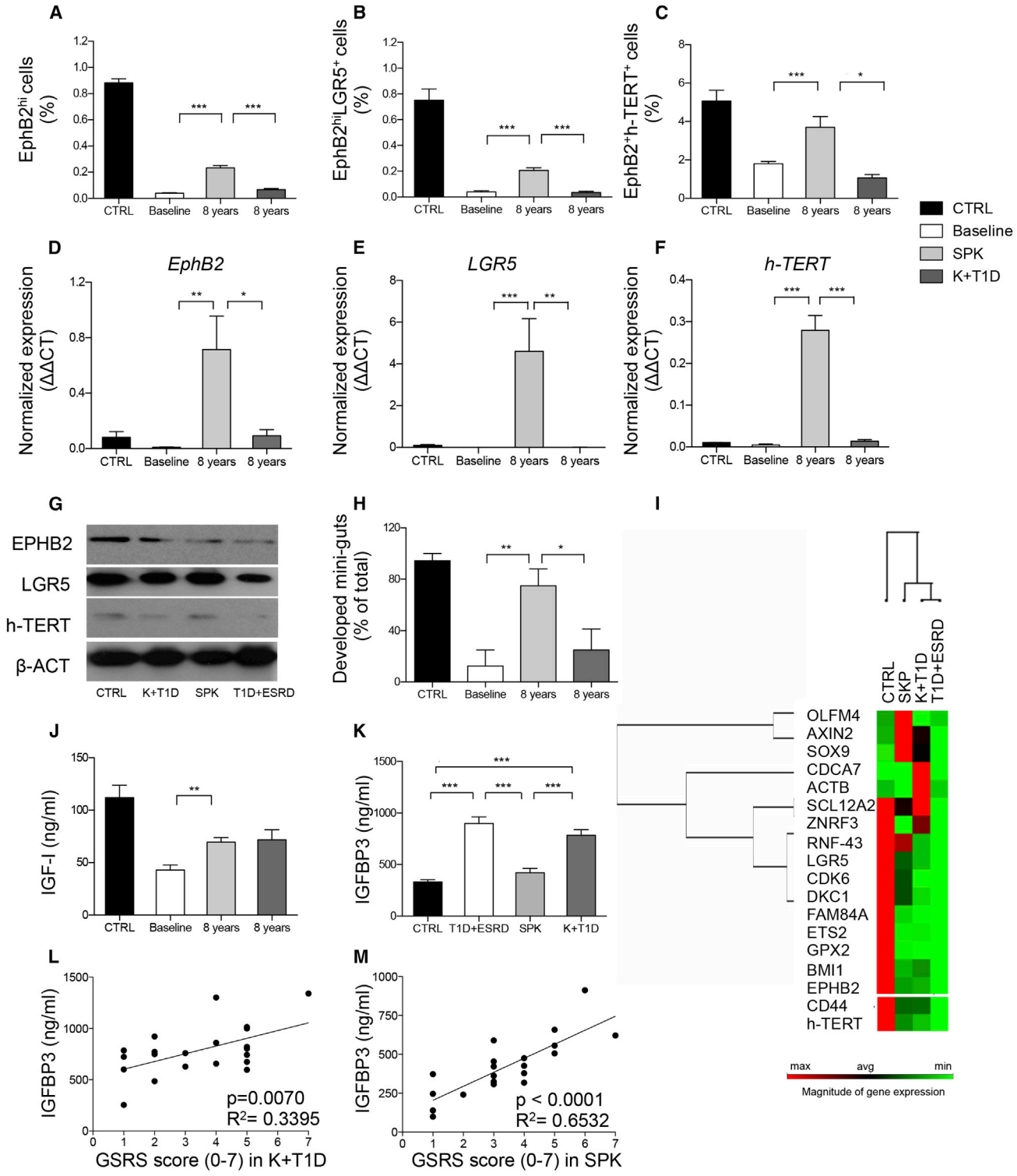

Figure 5. Treatment of Long-Standing T1D with SPK Replenishes CoSCs and Restores the CoSC Signature Profile and Mini-Gut Development through Restoration of Circulating IGF-I and IGFBP3

(A–C) Bar graphs depict results of flow cytometric analysis of EphB2^{hi+}, EphB2^{hi+}LGR5^{+}, and EphB2^{+}h-TERT^{+} cells obtained from isolated crypts in long-standing T1D (Baseline) or T1D+ESRD who underwent kidney+pancreas (SPK) or kidney alone (K+T1D) transplantation at 8 years of follow-up. n = 10 subjects per group were evaluated.

(D–F) Bar graphs depict normalized mRNA expression of intestinal stem cell markers *EphB2, LGR5,* and *h-TERT* measured by RT-PCR on isolated intestinal crypts obtained from long-standing T1D (Baseline) or T1D+ESRD who underwent kidney+pancreas (SPK) or kidney alone (K+T1D) transplantation at 8 years of

(legend continued on next page)

apoptotic-related caspase-mediated IGFBP3 activity. The expression of the survival factor beta-catenin (*CTNNB1*) was reduced in mini-guts generated from crypts of T1D+ESRD individuals as compared to those obtained from healthy subjects (Figure S3K) and was increased by the addition of IGF-I (Figure S3L), further supporting the concept of an apoptotic-related mechanism, whereby circulating IGFBP3 directly controls CoSCs (Movie S1).

Manipulation of the Circulating IGF-I/IGFBP3 Dyad Alters the Course of Diabetic Enteropathy in a Preclinical Model

In order to further demonstrate the relevance of IGF-I/IGFBP3 circulating factors in vivo, we tested the effects of IGF-I and IGFBP3 administration in a preclinical model of DE. After 8 weeks of chemically induced diabetes (using streptozotocin [STZ]), C57BL/6J (B6) mice showed a reduced number of crypts in the colorectal tissue (Figure 4E), which displayed increased depth (Figure 4F) and width in more than 70% of cases (Figures 4G, 4I1, 4I2, 4I4, and 4I5) and a reduced number of Aldh$^+$ cells (Figures 4H–4J). Interestingly, these mice showed increased serum levels of IGFBP3 and low levels of IGF-I, with lower murine insulin levels as compared to naive B6 (Figures S4A–S4C). Intraperitoneal (i.p.) administration of IGFBP3 in naive B6 mice resulted in a reduction in local crypt numbers (Figures 4E and 4I3), with the majority of crypts showing increased depth and width (Figures 4F, 4G, 4I3, and 4I6) and a significant reduction in Aldh$^+$ cells as compared to those of untreated mice (Figures 4H and 4J3). Those features were aggravated by IGFBP3 administration to STZ-treated B6 mice (Figures S4D–S4H), with evidence of decreases in weight (Figure S4I), CoSC loss (Figures S4J–S4L), and upregulated expression of *caspase 8* and *9* (Figures S4M and S4N). Administration of i.p. IGF-I in STZ-treated B6 mice only partially improved mucosa morphology and increased the number of crypts, which remained abnormal (Figure S4D, S4H1, and S4H2), and only partially restored the number of Aldh$^+$ cells (Figure S4G). Validation for successful administration of the injected compounds was performed by analysis of IGF-I/IGFBP3 peripheral levels 1 hr after their injection (Figures S4O and S4P). These observations confirmed that the peripheral IGF-I/IGFBP3 dyad controls CoSCs (Figure 4K).

Treatment of Long-Standing T1D with Simultaneous Pancreas-Kidney Transplantation Reverts Clinical and Morphological Features of DE

The gold standard treatment for long-standing T1D is simultaneous pancreas-kidney transplantation (SPK), which affords stable glycometabolic control, near-normalized risk factors, and prolonged survival (Table S4) (Fiorina et al., 2004, 2005; Folli et al., 2010; Secchi et al., 1998; Smets et al., 1999). However, individuals with T1D+ESRD are also treated with kidney transplantation alone but they remain diabetic (K+T1D) (Fiorina et al., 2001). A significant improvement in gastrointestinal symptoms was evident over time after SPK in our cohort of transplanted individuals, while the K+T1D group did not report any benefit (Figures S5A–S5C), suggesting that DE is reversible.

Treatment of Long-Standing T1D with SPK Reestablishes Intestinal Mucosa Morphology and Local Self-Renewal Properties

Analysis of intestinal mucosa samples showed a significant recovery in the structure of the epithelial compartment, with compensatory epithelial hyperplasia in the SPK group (Figures S5D1 and S5D2). Recovery of normal crypt histology and number was evident in the SPK group when long-standing T1D was successfully treated while none of these features were evident in individuals who received kidney transplant only and remained diabetic (Figures S5D1 and S5D2). Epithelial cell proliferation (MIB1$^+$ cells) increased after SPK over time as compared to baseline and K+T1D at each time point (Figures 4L–4M), with near-normalization of intestinal morphology, epithelial renewal, and neural features (Figures S5E–S5K). This demonstrates that treatment of long-standing T1D with SPK promoted recovery of intestinal epithelial repair and self-renewing properties.

Treatment of Long-Standing T1D Promotes Restoration of CoSCs

Treatment of long-standing T1D with SPK is associated with an increase in Aldh$^+$ cells (Figures 4N–4O) and EphB2$^+$ expression in the intestinal crypt (Figures 4P–4Q) and nearly normalizes the percentage of EphB2^{hi+}, EphB2$^+$h-TERT$^+$, and EphB2^{hi+} LGR5$^+$ cells in isolated intestinal crypts as compared to baseline (Figures 5A–5C). CoSC marker expression (Figures 5D–5G) and growth/morphology of mini-guts obtained from SPK individuals

follow-up. All samples were run in triplicate and normalized to expression of the housekeeping gene *ACTB* using the ΔΔCt method. n = 10 subjects per group were evaluated.

(G) WB analysis depicts the expression of EphB2, LGR5, and h-TERT in isolated intestinal crypts of the four groups at 8 years of follow-up. n = 5 subjects per group were evaluated.

(H) Bar graph depicts the percentages of developed mini-guts of the total at 8 days of culture of freshly isolated intestinal crypts obtained from long-standing T1D individuals (Baseline) or SPK and K+T1D subjects at 8 years of follow-up. n = 10 subjects per group were evaluated.

(I) Heatmap represents the CoSC signature marker transcriptomic profiling examined in freshly isolated intestinal crypts of CTRL, long-standing T1D individuals (T1D+ESRD), SPK, and K+T1D subjects at 8 years of follow-up. n = 10 subjects per group were evaluated.

(J) Bar graph represents IGF-I levels measured by ELISA in serum of the four groups of subjects at 8 years of follow-up. n = 10 subjects per group were evaluated.

(K) Bar graph depicts IGFBP3 levels measured by ELISA in serum of the four groups of subjects. n = 20 subjects per group were evaluated.

(L and M) Correlation between IGFBP3 serum levels and intestinal symptoms assessed using the GSRS questionnaire (0–7) in n = 20 subjects of K+T1D (L) and SPK (M) group. Analysis was conducted using ANOVA ($p < 0.05$) in comparing all groups. Data are expressed as mean ± SEM unless differently reported. *$p < 0.01$; **$p < 0.001$; ***$p < 0.0001$. See also Figures S5 and S6.

CoSC, colonic stem cell; T1D, type 1 diabetes; ESRD, end stage renal disease; CTRL, healthy subjects; SPK, simultaneous kidney-pancreas transplantation; EphB2, Ephrin B receptor 2; LGR5, leucine-rich repeat containing G protein-coupled receptor 5; RT-PCR, real-time polymerase chain reaction; ACTB, beta actin; K+T1D, kidney transplantation alone in type 1 diabetes; IGF-I, insulin-like growth factor 1; IGFBP3, insulin-like growth factor binding protein 3; SEM, standard error of the mean.

were nearly normalized as well (Figure 5H, Figures S6A1–S6A6). Transcriptome analysis revealed that SPK nearly restored the expression of CoSCs markers and pathways involved in preserving CoSCs integrity (Figure 5I, Figure S6B). Taken together, our data suggest that treatment of long-standing T1D with SPK promotes restoration of CoSCs.

Treatment of Long-Standing T1D with SPK Restores Circulating IGF-I and IGFBP3

Broad proteomic analysis and targeted immunoassay revealed a near-normalization of IGFBP3 and IGF-I serum levels after SPK (Figures 5J and 5K) in association with a nearly reestablished expression of *IGF-IR* (Figure S6C). These results were not evident in the K+T1D group, who showed low levels of IGF-I (Figure 5J) and *IGF-IR* expression (Figure S6C) and only a partial recovery in their IGFBP profile (Figure S6D). A significant correlation between IGFBP3 serum levels and intestinal symptoms in both SPK and K+T1D groups, but more evident in the latter, confirmed that the restoration of IGFBP3 levels is associated with an improvement in DE (Figures 5L and 5M). Treatment of long-standing T1D with SPK ameliorates DE via a glucose-associated restoration of the circulating IGF-I/IGFBP3 dyad.

The Ecto-TMEM219 Recombinant Protein Abrogates IGFBP3-Mediated Mini-Gut Destruction In Vitro and Preserves CoSCs In Vivo in a Murine Model of DE

In order to further demonstrate the IGFBP3-mediated detrimental effects on CoSCs, we generated a recombinant protein based on the 161-amino-acid TMEM219 extracellular domain (ecto-TMEM219) with >90% purity. Addition of ecto-TMEM219 (2:1 molar ratio with IGFBP3) to crypts obtained from CTRL and cultured with IGFBP3 abrogated the pro-apoptotic effect of IGFBP3 on mini-guts and preserved the regenerative properties of crypts to generate mini-guts (Figure 6A). The expression of the CoSC marker EphB2 was significantly recovered in mini-guts cultured with IGFBP3 and ecto-TMEM219 (Figure 6B), emphasizing a favorable effect in preserving CoSCs, which was also confirmed in high-glucose-cultured mini-guts (Figure 6A). Moreover, analysis of *caspase 8* and *9* by RT-PCR documented a net decrease in their expression when ecto-TMEM219 was added to IGFBP3-cultured mini-guts as compared to IGFBP3 alone (Figures 6C and 6D). We then treated STZ-B6 mice with ecto-TMEM219 and observed improved mucosa morphology with recovered number, depth, and width of crypts (Figures 6E and 6G). Administration of ecto-TMEM219 was associated with an increase in mouse body weight as compared to STZ-treated B6 (Figure 6H), with significant regain of CoSCs (Figures 6I–6K), a decreased expression of *caspase 8* and *9* (Figures 6L and 6M), and a reestablishment of circulating IGFBP3 levels (Figure 6N), therefore suggesting a curative potential of ecto-TMEM219 in a therapeutic scenario.

DISCUSSION

DE represents a clinically relevant complication in individuals with T1D, as it is associated with lower quality of life, malnutrition, and malabsorbtion (Bytzer et al., 2002; Faraj et al., 2007; Talley et al., 2001). Particularly, in individuals with long-standing T1D (T1D+ESRD), intestinal disorders occur with high frequency and severity (Cano et al., 2007; Wu et al., 2004), resulting in body mass loss and cachexia (Pupim et al., 2005), indicating that enteropathy is an important complication of long-standing T1D (Atkinson et al., 2014; Pambianco et al., 2006). Our results demonstrate that individuals with long-standing T1D experienced severe intestinal disorders and that these clinical conditions are associated with alterations of the intestinal mucosa, with reduced proliferation of intestinal epithelial cells and with signs of neural degeneration. Similar features have also been reported in rodent models of T1D and DE (Domènech et al., 2011). Our data link DE to a defect in CoSCs and implicate IGFBP3 as having an important role in the maintenance of intestinal epithelium homeostasis. While hyperglycemia is a prominent feature of T1D, our in vitro studies suggest that this feature cannot fully explain DE and that circulating factors may play an important role. Proteomic analysis led to the identification of IGF-I as an enterotrophic factor involved in the homeostasis of CoSCs. We then confirmed that IGF-I and IGFBP3 control CoSCs and that this axis is dysfunctional in long-standing T1D. Our data indicate that IGF-I acts as a circulating enterotrophic factor that promotes crypt growth and controls CoSCs through IGF-IR, while IGFBP3 can block IGF-I signaling by binding circulating IGF-I and reducing its bioavailability. In addition, and most importantly, we showed that IGFBP3 acts through a pro-apoptotic IGF-I-independent mechanism on CoSCs, which we demonstrated express TMEM219 (the IGFBP3 receptor), thereby inducing the failure of mini-gut growth. This latter effect is caspase 8 and 9 mediated and TMEM219 dependent; indeed, the absence of the IGFBP3 receptor (TMEM219) on CoSCs greatly diminished high-glucose-associated CoSC injuries. T1D together with starvation and cachexia are characterized by low circulating IGF-I levels (Bondy et al., 1994; Giustina et al., 2015) due to reduced hepatic IGF-I release, which is controlled and stimulated by endogenous insulin (Le Roith, 1997; Sridhar and Goodwin, 2009). More importantly, hyperglycemia appeared to have a direct effect on hepatic synthesis and release of IGFBP3. IGFBP3 may thus act as a hepatic hormone that reduces intestinal absorptive capacity during hyperglycemia. Interestingly, SPK provided a proof of concept to our hypothesis and supported our findings regarding the existence of circulating factors that control CoSCs. The striking improvement of clinical and functional features of DE that we observed in our study, associated with replenishment of CoSCs and with restoration of the circulating IGF-I and IGFBP3, strengthens our hypothesis. Finally, the newly generated ecto-TMEM219 recombinant protein improved DE in diabetic mice in vivo and restored the ability of mini-guts to grow normally in vitro, thus confirming the role of IGFBP3 in controlling CoSCs and paving the way for a potential therapeutic strategy (Movie S1). In summary, our study shows that an IGFBP3-mediated disruption of CoSCs linked to hyperglycemia is evident in DE. We suggest that circulating IGF-I/IGFBP3 represents a hormonal dyad that controls CoSCs and a therapeutic target for individuals with intestinal disorders caused by diabetes mellitus of long duration (Bondy et al., 1994; Bortvedt and Lund, 2012; Boucher et al., 2010).

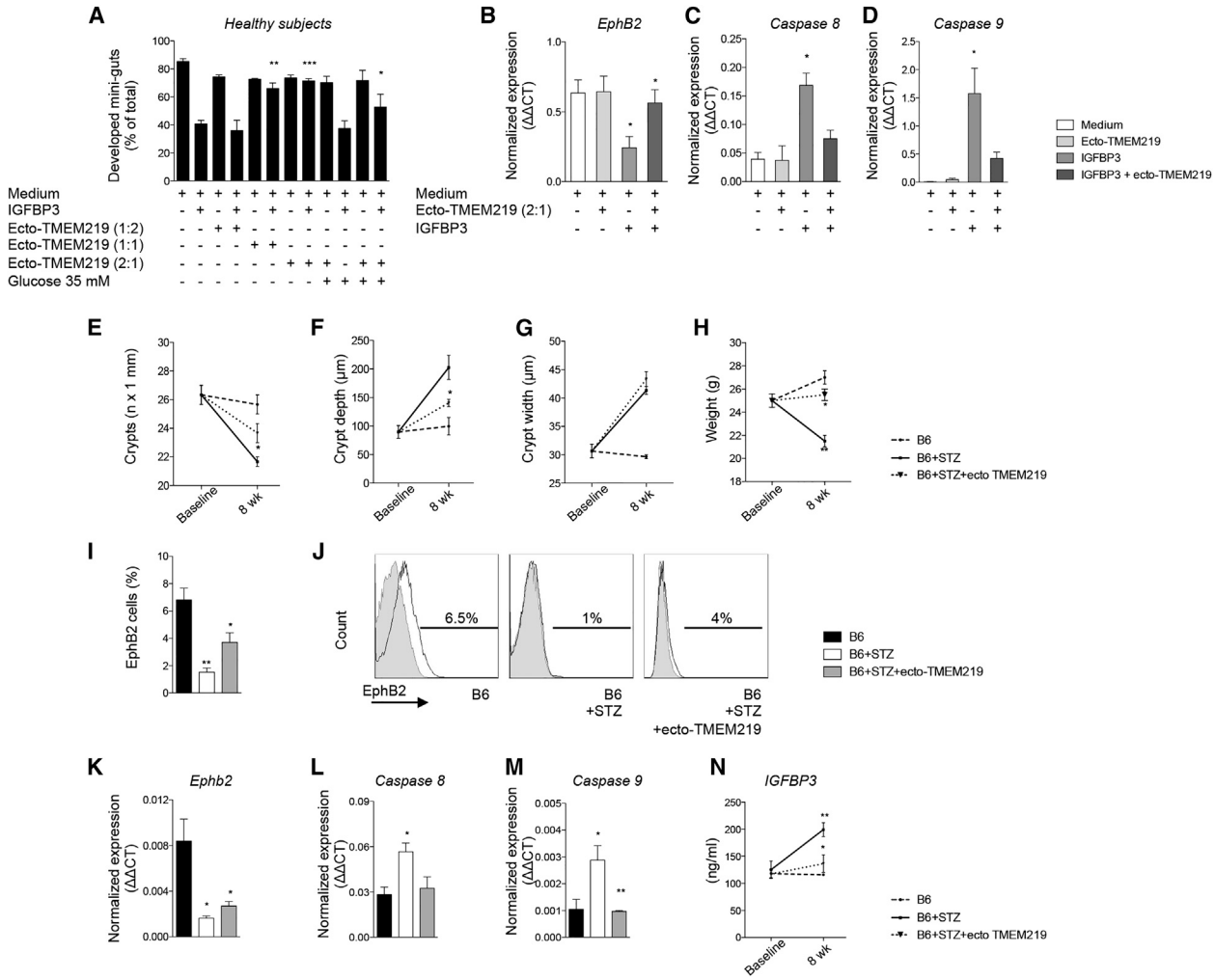

Figure 6. Treatment with the Newly Generated Recombinant Protein Ecto-TMEM219 (Ecto-TMEM219) Abrogates IGFBP3-Mediated Mini-Gut Destruction and Preserves CoSCs in a Preclinical Model

(A) Bar graph grouping percentages of developed mini-guts of the total obtained from healthy subjects in different conditions and showing the effect of ecto-TMEM219 at various concentrations (1:2, 1:1, and 2:1 molar ratio as compared to IGFBP3) in IGFBP3-treated mini-guts and in those exposed to high glucose. The p values are relative to baseline conditions.

(B) Bar graph representing normalized mRNA expression of EphB2 in crypts isolated from healthy subjects cultured in the presence of IGFBP3 and ecto-TMEM219+IGFBP3. Experiments were performed in triplicate.

(C and D) Bar graphs representing normalized mRNA expression of caspases 8 and 9 in crypts isolated from healthy subjects cultured in the presence of IGFBP3 and ecto-TMEM219+IGFBP3. Experiments were performed in triplicate.

(E–G) Line graphs reporting the number of crypts (E), depth of crypts (F), and width of crypts (G) assessed on intestinal lower tract sections harvested at baseline and after 8 weeks from STZ-treated B6 mice developing DE (B6+STZ), naive B6 (B6), and STZ-B6 mice treated with ecto-TMEM219. STZ, streptozoticin-treated. n = 3 mice per group were evaluated.

(H) Line graph reporting the weight at baseline and after 8 weeks of STZ-treated B6 mice developing DE (B6+STZ), naive B6 (B6), and STZ-treated B6 mice developing DE treated with ecto-TMEM219. STZ, streptozoticin-treated. n = 3 mice per group were evaluated.

(I) Bar graph representing results of flow cytometric analysis of $EphB2^+$ cells isolated from intestinal samples collected from naive B6 mice, STZ-treated B6 mice, and STZ-B6 mice treated with ecto-TMEM219 at 8 weeks.

(J) Representative flow histograms of $EphB2^+$ cells isolated from crypts isolated from naive B6 mice, STZ-treated B6 mice, and STZ-B6 mice treated with ecto-TMEM219 at 8 weeks. n = 3–5 mice per group were evaluated.

(K) Bar graph representing normalized mRNA expression of *Ephb2* in intestinal samples collected from naive B6 mice, STZ-treated B6 mice, and STZ-B6 mice treated with ecto-TMEM219 at 8 weeks.

(L and M) Bar graph representing normalized mRNA expression of *caspase 8* (L) and *caspase 9* (M) in intestinal samples collected from naive B6 mice, STZ-treated B6 mice, and STZ-B6 mice treated with ecto-TMEM219 at 8 weeks.

(N) Line graph representing murine IGFBP3 circulating levels measured in naive B6 mice (B6), STZ-treated B6 mice (B6+STZ), and B6+STZ mice treated with ecto-TMEM219 at baseline and after 8 weeks. n = 3–5 mice per group. Data are expressed as mean ± SEM unless differently reported. *p < 0.01; **p < 0.001; ***p < 0.0001. See also Figure S6.

STZ, streptozoticin-treated; B6, C57BL/6J mice; IGF-I, insulin-like growth factor 1; IGFBP3, insulin-like growth factor binding protein 3; CoSC, colonic stem cell; EphB2, Ephrin B receptor 2; T1D, type 1 diabetes; ESRD, end stage renal disease; CTRL, healthy subjects; RT-PCR, real-time polymerase chain reaction; ACTB, beta actin.

EXPERIMENTAL PROCEDURES

60 individuals with long-standing T1D (T1D+ESRD) registered on the waiting list for SPK were enrolled in the study and compared with 20 healthy subjects matched for age and gender (CTRL). Assessment of gastrointestinal symptoms, intestinal motility, and intestinal mucosa pathology defined DE. CoSCs were identified on colonic purified crypts based on the expression of CoSC-specific markers (flow cytometry, RT-PCR, WB, transcriptome profiling). CoSC self-renewal properties were assessed by evaluation of the percentage of in vitro developed mini-guts and by the characterization of their expression of cell lineage markers in different conditions (Figures S6E–S6I and S6J). Interventional studies included the use of recombinant human IGF-I, recombinant human IGFBP3, and anti-IGF-IR in vitro in mini-gut assay and in vivo in murine models of DE. Animal studies were conducted on B6 mice purchased from the Jackson Laboratory, in accordance with institutional guidelines (Harvard Medical School Institutional Animal Care and Use Committee). Mice were rendered diabetic with STZ injection and development of DE was assessed after 8 weeks (via intestinal pathology, CoSCs flow cytometry, and RT-PCR). The recombinant protein ecto-TMEM219 for in vitro and in vivo studies (161 amino acids, 18.2 kDa) was generated using *E. coli* for expression and synthesis, while purity was tested by SDS-PAGE and WB (Figures S6K and S6L). The co-injection of IGFBP3 and ecto-TMEM219 prevented the increase of IGFBP3 peripheral levels and implies the binding of ecto-TMEM219 with IGFBP3 (Figure S6M). Broad serum proteomic analysis was used to detect circulating factors that may regulate CoSCs and candidate factors were then tested in the in vitro mini-gut assay (Table S5). Peripheral levels of IGF-I and IGFBP3 were confirmed in human and murine studies using targeted immunoassays. Detailed methods and statistical analysis are described in the Supplemental Information. The study was approved by the Institutional Review Board of Istituto di Ricovero e Cura a Carattere Scientifico Ospedale San Raffaele, Milano, Italy (Enteropathy-Pancreas KidneyTransplantation/01 Secchi/Fiorina).

SUPPLEMENTAL INFORMATION

Supplemental Information for this article includes six figures, five tables, one movie, and Supplemental Experimental Procedures and can be found with this article online at http://dx.doi.org/10.1016/j.stem.2015.07.010.

AUTHOR CONTRIBUTIONS

F.D. and S.L.R. designed the study, performed experiments, analyzed data, and wrote the paper; A. Maestroni, E.O., M.B.N., S.T., R.B., and A.V. performed experiments and analyzed data; G.F. and A. Marando helped with histology and electron microscopy analysis; R.F. and L.A. helped with sample collection; A.A. performed proteomic analysis and provided suggestions; R.M. and D.C. helped with immunostaining; E.V. helped with sample collection; P.J. and D.B. helped with mini-gut experiments and edited the paper; C.S. coordinated research; F.F. and A.S. designed research and edited the paper; and P.F. conceived the idea, designed the study, and wrote and edited the paper.

ACKNOWLEDGMENTS

We thank Protein Micro Sequencing Facility, Ospedale San Raffaele, Milan, Italy for proteomic analysis and Gabriella Becchi (Department of Biomedical, Biotechnological and Translational Sciences, Unit of Pathology, University of Parma, Parma) for immunohistochemistry studies. F.D. is a recipient of an Italian Scientists and Scholars of North America Foundation (ISSNAF)-Fondazione Marche Fellowship. P.F., C.S., and A.S. are recipients of a Minister of Health of Italy grant RF-2010-2314794. P.F. received a Minister of Health of Italy grant RF-2010-233119. P.F. is the recipient of an ADA mentor-based fellowship and an EFSD/Sanofi European Research Programme and is supported by an American Heart Association (AHA) Grant-in-Aid. R.B. is supported by an AST fellowship. M.B.N. is supported by an ADA mentor-based fellowship. D.B. is supported by RO1DK084056 and P30DK034854. F.F. is on sabbatical leave from the University of Texas Health Science Center, San Antonio, TX, USA at Unicamp, Campinas, Brazil and he is supported by FAPESP, CNPq.

Received: December 15, 2014
Revised: June 2, 2015
Accepted: July 19, 2015
Published: October 1, 2015

REFERENCES

Atkinson, M.A., Eisenbarth, G.S., and Michels, A.W. (2014). Type 1 diabetes. Lancet *383*, 69–82.

Barker, N. (2014). Adult intestinal stem cells: critical drivers of epithelial homeostasis and regeneration. Nat. Rev. Mol. Cell Biol. *15*, 19–33.

Baxter, R.C. (2013). Insulin-like growth factor binding protein-3 (IGFBP-3): Novel ligands mediate unexpected functions. J. Cell Commun. Signal. *7*, 179–189.

Bondy, C.A., Underwood, L.E., Clemmons, D.R., Guler, H.P., Bach, M.A., and Skarulis, M. (1994). Clinical uses of insulin-like growth factor I. Ann. Intern. Med. *120*, 593–601.

Bortvedt, S.F., and Lund, P.K. (2012). Insulin-like growth factor 1: common mediator of multiple enterotrophic hormones and growth factors. Curr. Opin. Gastroenterol. *28*, 89–98.

Boucher, J., Macotela, Y., Bezy, O., Mori, M.A., Kriauciunas, K., and Kahn, C.R. (2010). A kinase-independent role for unoccupied insulin and IGF-1 receptors in the control of apoptosis. Sci. Signal. *3*, ra87.

Breault, D.T., Min, I.M., Carlone, D.L., Farilla, L.G., Ambruzs, D.M., Henderson, D.E., Algra, S., Montgomery, R.K., Wagers, A.J., and Hole, N. (2008). Generation of mTert-GFP mice as a model to identify and study tissue progenitor cells. Proc. Natl. Acad. Sci. USA *105*, 10420–10425.

Bytzer, P., Talley, N.J., Hammer, J., Young, L.J., Jones, M.P., and Horowitz, M. (2002). GI symptoms in diabetes mellitus are associated with both poor glycemic control and diabetic complications. Am. J. Gastroenterol. *97*, 604–611.

Camilleri, M. (2007). Clinical practice. Diabetic gastroparesis. N. Engl. J. Med. *356*, 820–829.

Cano, A.E., Neil, A.K., Kang, J.Y., Barnabas, A., Eastwood, J.B., Nelson, S.R., Hartley, I., and Maxwell, D. (2007). Gastrointestinal symptoms in patients with end-stage renal disease undergoing treatment by hemodialysis or peritoneal dialysis. Am. J. Gastroenterol. *102*, 1990–1997.

Carlone, D.L., and Breault, D.T. (2012). Tales from the crypt: the expanding role of slow cycling intestinal stem cells. Cell Stem Cell *10*, 2–4.

Carpentino, J.E., Hynes, M.J., Appelman, H.D., Zheng, T., Steindler, D.A., Scott, E.W., and Huang, E.H. (2009). Aldehyde dehydrogenase-expressing colon stem cells contribute to tumorigenesis in the transition from colitis to cancer. Cancer Res. *69*, 8208–8215.

Domènech, A., Pasquinelli, G., De Giorgio, R., Gori, A., Bosch, F., Pumarola, M., and Jiménez, M. (2011). Morphofunctional changes underlying intestinal dysmotility in diabetic RIP-I/hIFNβ transgenic mice. Int. J. Exp. Pathol. *92*, 400–412.

Faraj, J., Melander, O., Sundkvist, G., Olsson, R., Thorsson, O., Ekberg, O., and Ohlsson, B. (2007). Oesophageal dysmotility, delayed gastric emptying and gastrointestinal symptoms in patients with diabetes mellitus. Diabet. Med. *24*, 1235–1239.

Feldman, M., and Schiller, L.R. (1983). Disorders of gastrointestinal motility associated with diabetes mellitus. Ann. Intern. Med. *98*, 378–384.

Fiorina, P., La Rocca, E., Venturini, M., Minicucci, F., Fermo, I., Paroni, R., D'Angelo, A., Sblendido, M., Di Carlo, V., Cristallo, M., et al. (2001). Effects of kidney-pancreas transplantation on atherosclerotic risk factors and endothelial function in patients with uremia and type 1 diabetes. Diabetes *50*, 496–501.

Fiorina, P., Folli, F., D'Angelo, A., Finzi, G., Pellegatta, F., Guzzi, V., Fedeli, C., Della Valle, P., Usellini, L., Placidi, C., et al. (2004). Normalization of multiple hemostatic abnormalities in uremic type 1 diabetic patients after kidney-pancreas transplantation. Diabetes *53*, 2291–2300.

Fiorina, P., Venturini, M., Folli, F., Losio, C., Maffi, P., Placidi, C., La Rosa, S., Orsenigo, E., Socci, C., Capella, C., et al. (2005). Natural history of kidney graft survival, hypertrophy, and vascular function in end-stage renal disease type 1

diabetic kidney-transplanted patients: beneficial impact of pancreas and successful islet cotransplantation. Diabetes Care *28*, 1303–1310.

Folli, F., Guzzi, V., Perego, L., Coletta, D.K., Finzi, G., Placidi, C., La Rosa, S., Capella, C., Socci, C., Lauro, D., et al. (2010). Proteomics reveals novel oxidative and glycolytic mechanisms in type 1 diabetic patients' skin which are normalized by kidney-pancreas transplantation. PLoS ONE *5*, e9923.

Giustina, A., Berardelli, R., Gazzaruso, C., and Mazziotti, G. (2015). Insulin and GH-IGF-I axis: endocrine pacer or endocrine disruptor? Acta Diabetol. *52*, 433–443.

Gracz, A.D., Fuller, M.K., Wang, F., Li, L., Stelzner, M., Dunn, J.C., Martin, M.G., and Magness, S.T. (2013). Brief report: CD24 and CD44 mark human intestinal epithelial cell populations with characteristics of active and facultative stem cells. Stem Cells *31*, 2024–2030.

Hughes, K.R., Sablitzky, F., and Mahida, Y.R. (2011). Expression profiling of Wnt family of genes in normal and inflammatory bowel disease primary human intestinal myofibroblasts and normal human colonic crypt epithelial cells. Inflamm. Bowel Dis. *17*, 213–220.

Jung, P., Sato, T., Merlos-Suárez, A., Barriga, F.M., Iglesias, M., Rossell, D., Auer, H., Gallardo, M., Blasco, M.A., Sancho, E., et al. (2011). Isolation and in vitro expansion of human colonic stem cells. Nat. Med. *17*, 1225–1227.

Le Roith, D. (1997). Seminars in medicine of the Beth Israel Deaconess Medical Center. Insulin-like growth factors. N. Engl. J. Med. *336*, 633–640.

Medema, J.P., and Vermeulen, L. (2011). Microenvironmental regulation of stem cells in intestinal homeostasis and cancer. Nature *474*, 318–326.

Merlos-Suárez, A., Barriga, F.M., Jung, P., Iglesias, M., Céspedes, M.V., Rossell, D., Sevillano, M., Hernando-Momblona, X., da Silva-Diz, V., Muñoz, P., et al. (2011). The intestinal stem cell signature identifies colorectal cancer stem cells and predicts disease relapse. Cell Stem Cell *8*, 511–524.

Muñoz, J., Stange, D.E., Schepers, A.G., van de Wetering, M., Koo, B.K., Itzkovitz, S., Volckmann, R., Kung, K.S., Koster, J., Radulescu, S., et al. (2012). The Lgr5 intestinal stem cell signature: robust expression of proposed quiescent '+4' cell markers. EMBO J. *31*, 3079–3091.

Pambianco, G., Costacou, T., Ellis, D., Becker, D.J., Klein, R., and Orchard, T.J. (2006). The 30-year natural history of type 1 diabetes complications: the Pittsburgh Epidemiology of Diabetes Complications Study experience. Diabetes *55*, 1463–1469.

Pupim, L.B., Heimbürger, O., Qureshi, A.R., Ikizler, T.A., and Stenvinkel, P. (2005). Accelerated lean body mass loss in incident chronic dialysis patients with diabetes mellitus. Kidney Int. *68*, 2368–2374.

Sato, T., and Clevers, H. (2013). Growing self-organizing mini-guts from a single intestinal stem cell: mechanism and applications. Science *340*, 1190–1194.

Sato, T., Stange, D.E., Ferrante, M., Vries, R.G., Van Es, J.H., Van den Brink, S., Van Houdt, W.J., Pronk, A., Van Gorp, J., Siersema, P.D., and Clevers, H. (2011). Long-term expansion of epithelial organoids from human colon, adenoma, adenocarcinoma, and Barrett's epithelium. Gastroenterology *141*, 1762–1772.

Secchi, A., Caldara, R., La Rocca, E., Fiorina, P., and Di Carlo, V. (1998). Cardiovascular disease and neoplasms after pancreas transplantation. Lancet *352*, 65, author reply 66.

Smets, Y.F., Westendorp, R.G., van der Pijl, J.W., de Charro, F.T., Ringers, J., de Fijter, J.W., and Lemkes, H.H. (1999). Effect of simultaneous pancreas-kidney transplantation on mortality of patients with type-1 diabetes mellitus and end-stage renal failure. Lancet *353*, 1915–1919.

Sridhar, S.S., and Goodwin, P.J. (2009). Insulin-insulin-like growth factor axis and colon cancer. J. Clin. Oncol. *27*, 165–167.

Stange, D.E., and Clevers, H. (2013). Concise review: the yin and yang of intestinal (cancer) stem cells and their progenitors. Stem Cells *31*, 2287–2295.

Talley, N.J., Young, L., Bytzer, P., Hammer, J., Leemon, M., Jones, M., and Horowitz, M. (2001). Impact of chronic gastrointestinal symptoms in diabetes mellitus on health-related quality of life. Am. J. Gastroenterol. *96*, 71–76.

The Diabetes Control and Complications Trial Research Group (1993). The effect of intensive treatment of diabetes on the development and progression of long-term complications in insulin-dependent diabetes mellitus. N. Engl. J. Med. *329*, 977–986.

van der Flier, L.G., and Clevers, H. (2009). Stem cells, self-renewal, and differentiation in the intestinal epithelium. Annu. Rev. Physiol. *71*, 241–260.

Williams, A.C., Smartt, H., H-Zadeh, A.M., Macfarlane, M., Paraskeva, C., and Collard, T.J. (2007). Insulin-like growth factor binding protein 3 (IGFBP-3) potentiates TRAIL-induced apoptosis of human colorectal carcinoma cells through inhibition of NF-kappaB. Cell Death Differ. *14*, 137–145.

Wu, M.J., Chang, C.S., Cheng, C.H., Chen, C.H., Lee, W.C., Hsu, Y.H., Shu, K.H., and Tang, M.J. (2004). Colonic transit time in long-term dialysis patients. Am. J. Kidney Dis. *44*, 322–327.

Zeki, S.S., Graham, T.A., and Wright, N.A. (2011). Stem cells and their implications for colorectal cancer. Nat. Rev. Gastroenterol. Hepatol. *8*, 90–100.

Zhao, J., Yang, J., and Gregersen, H. (2003). Biomechanical and morphometric intestinal remodelling during experimental diabetes in rats. Diabetologia *46*, 1688–1697.

Ziskin, J.L., Dunlap, D., Yaylaoglu, M., Fodor, I.K., Forrest, W.F., Patel, R., Ge, N., Hutchins, G.G., Pine, J.K., Quirke, P., et al. (2013). In situ validation of an intestinal stem cell signature in colorectal cancer. Gut *62*, 1012–1023.